Electronic Supplementary Material (ESI) for Journal of Materials Chemistry A.


# Supporting Information

## Nitrogen Doped $NiS_2$ Nanoarray with Enhanced Electrocatalytic Activity for Water Oxidation

*Jinhui Hao, Wenshu Yang, Jianwen Hou, Baodong Mao, Zhipeng Huang, and Weidong Shi**

### Experimental Section

*Materials*:

$Ni(NO_3)_2$•$6H_2O$, $NH_3$•$H_2O$ and sulphur powder were purchased from Sinopharm Chemical Reagent Co. Ltd. (Shanghai, China). The carbon paper (CP) were purchased from Shanghai Hesen Co. Ltd. (Shanghai, China). Other reagents were of analytical grade and were used as received.

*Synthesis of $Ni(OH)_2$ and N doped $NiS_2$*:

The $Ni(OH)_2$ was synthesized through a simple hydrothermal reaction. Briefly, 60 mg $Ni(NO_3)_2$•$6H_2O$ was dissolved in 10 mL water to form a homogeneous solution. A piece of CP (1 cm×4 cm) was immersed into above solution and then 0.6 mL $NH_3$•$H_2O$ was added. The mixture was transferred to a Teflon-lined autoclave and kept at 140 $^oC$ for 12 h. After being washed with deionized water and ethanol several times, the product was dried at room temperature. This obtained $Ni(OH)_2$ product was designated as $N_1$-$Ni(OH)_2$. When the amount of ammonium hydroxide were 1.2 and 2.4 mL, the obtained $Ni(OH)_2$ products were donated as $N_2$-$Ni(OH)_2$ and $N_3$-$Ni(OH)_2$.

The pure $Ni(OH)_2$ (donated as $N_0$-$Ni(OH)_2$) was synthesized according to the literature.[1]

In a typical synthesis of N doped $NiS_2$, the $N_2$-$Ni(OH)_2$ was annealed with sulphur powder. The $N_2$-$Ni(OH)_2$ and sulphur powder (200 mg) were placed separately in a fused silica tube, and sulphur powder was at the upstream side. Then the fused silica tube was heated to 400 $^oC$ with a heating rate of 10 °C/min and kept for 1 h under $N_2$. The obtained product was donated as $N_2$-$NiS_2$-400. When the sulfuration temperatures were 500 and 600 $^oC$, the final products were donated as $N_2$-$NiS_2$-500 and $N_2$-$NiS_2$-600.

*Characterization*:

XRD spectra were obtained using a D8 ADVANCE diffractometer (Bruker, Germany) using Cu Kα (1.5406 Å) radiation. SEM images were inspected on a Hitachi S-4800. XPS measurements were performed on an ESCALAB MKII spectrometer (VG Co., United Kingdom) with Al Kα X-ray radiation as the X-ray source for excitation.

*Electrochemical Measurements*:

All measurements were carried out in a three-electrode electrochemical cell at room temperature with a CHI 614D electrochemical workstation. The obtained N doped $NiS_2$-CP was directly used as the working electrode, while a Pt electrode as the counter electrode and a mercury/mercury oxide electrode (MOE) as the reference electrode. For preparation of the $RuO_2$ on CP, the $RuO_2$ was dispersed in ethanol to achieve a concentration of 1 mg $mL^{-1}$ with 4 wt% polytetrafluoroethylene. After sonication for 30 minutes, 250 μL of the $RuO_2$ ink was drop-dried onto a 1 cm × 1 cm

CP (loading 0.25 mg $cm^{-2}$). The potential was calibrated with respect to reversible hydrogen electrode potential (RHE), which was determined by a Pt/C electrode as the working electrode in electrolyte saturated with the high purity $H_2$. Before the electrochemical measurement, the electrolyte (1.0 M KOH) was degassed by bubbling argon for 30 min. EIS spectra were performed at 1.53 V vs. RHE in the frequency range of $10^{-2}$–$10^{6}$ Hz. The volume of $O_2$ during a potentiostatic electrolysis experiment was monitored by the water displacement method.[2]

*Turnover frequency (TOF) calculation* [3]:

$$TOF = \frac{J \times A}{4 \times F \times m} \tag{1}$$

*J* is the current density. *A* is the area of the carbon fiber paper electrode. *F* is the faraday constant (96485 *C/mol*). *m* is the number of moles of the active materials that are deposited onto the carbon fiber paper.

*DFT calculation*:

The electronic properties of N doped $NiS_2$ were investigated by density functional theory (DFT) calculation using the CASTEP (Cambridge Serial Total Energy Package) package.[4] The wave functions of the valence electrons were expanded in a plane wave basis set with k-vectors within a specified energy cutoff (300 eV). A 2×3×1 Monkhorst-Pack k-point mesh was employed. The unit cell with a slab along the (001) direction was applied in the calculation. All of the structures were fully optimized and relaxed to the ground state.

The OER process is assumed to involve four elementary reaction steps[5]:

$$H_2O + * \rightarrow HO^* + H^+ + e^- \tag{a}$$

$$HO^* \rightarrow O^* + H^+ + e^- \quad \text{(b)}$$

$$O^* + H_2O \rightarrow HOO^* + H^+ + e^- \quad \text{(c)}$$

$$OOH^* \rightarrow * + O_2 + H^+ + e^- \quad \text{(d)}$$

where * and *M** represent an active site and an adsorbed intermediate on the surface, respectively.

The free energy of the adsorbed state of each step was calculated as[5]:

$$\Delta G_a = E(HO^*) - E(^*) - E_{H_2O} + 1/2\, E_{H_2} + (\Delta ZPE - T\Delta S)_a - eU \quad (2)$$

$$\Delta G_b = E(O^*) - E(HO^*) + 1/2\, E_{H_2} + (\Delta ZPE - T\Delta S)_b - eU \quad (3)$$

$$\Delta G_c = E(HOO^*) - E(O^*) - E_{H_2O} + 1/2\, E_{H_2} + (\Delta ZPE - T\Delta S)_c - eU \quad (4)$$

$$\Delta G_d = E(^*) - E(HOO^*) + E_{O_2} + 1/2\, E_{H_2} + (\Delta ZPE - T\Delta S)_d - eU \quad (5)$$

where *E(*)*, *E(HO*)*, *E(O*)*, and *E(HOO*)* are the energies of the pure surface and the adsorbed surfaces with HO*, O*, and HOO* , respectively. $E_{H2O}$ and $E_{H2}$ are the computed energies for the sole $H_2O$ and $H_2$ molecules, respectively. The total free energy (ΔG) to form one molecule of $O_2$ was fixed at the value of 4.92 eV. *U* (vs. RHE) is the electrode potential used for changing all the free-energy steps into downhill.

To evaluate the ΔG on the (001) surface, we sampled five active sites, involving Ni-0, Ni-1, Ni-2, Ni-3, and Ni-4 site (Figure S19).

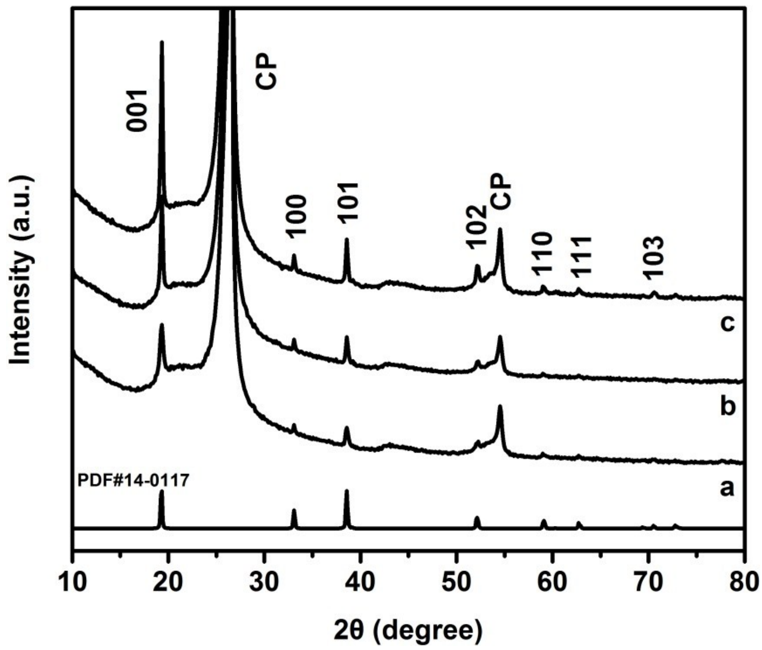


**Figure S1.** XRD patterns of $N_1$-$Ni(OH)_2$ (a), $N_2$-$Ni(OH)_2$ (b), and $N_3$-$Ni(OH)_2$ (c).

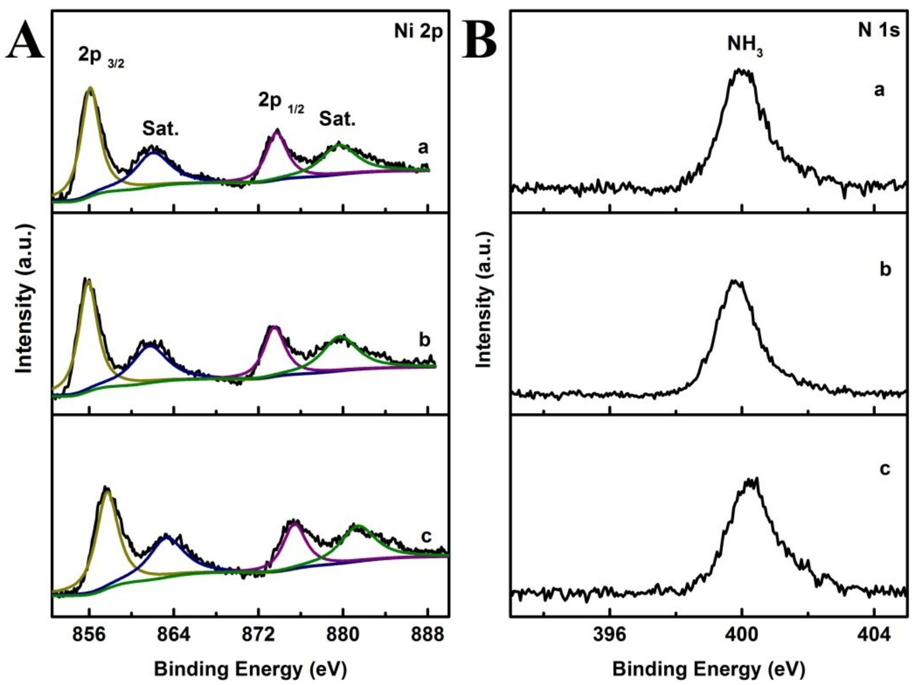


**Figure S2.** XPS spectra of $N_1$-$Ni(OH)_2$ (a), $N_2$-$Ni(OH)_2$ (b), and $N_3$-$Ni(OH)_2$ (c).

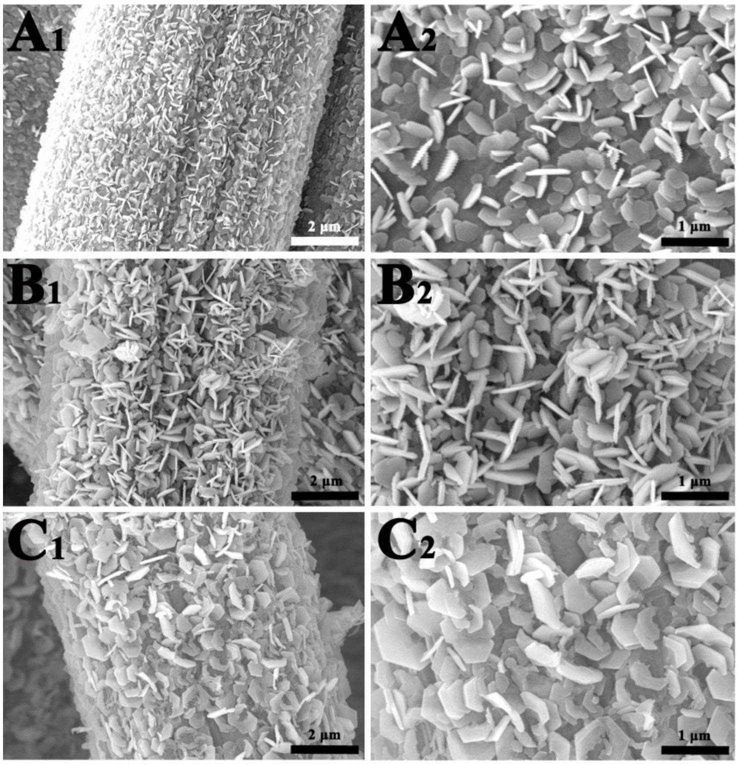


**Figure S3.** SEM images of $N_1$-$Ni(OH)_2$ (A), $N_2$-$Ni(OH)_2$ (B), and $N_3$-$Ni(OH)_2$ (C).

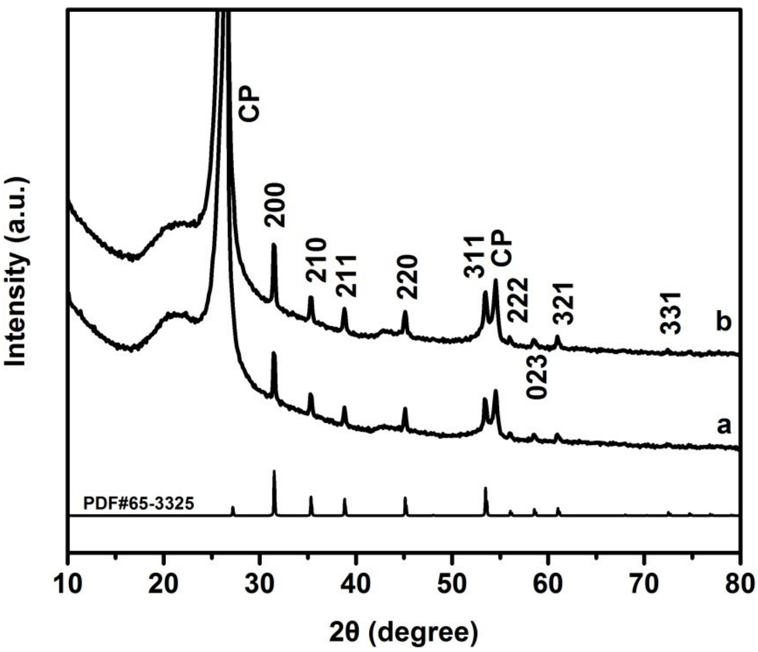


**Figure S4.** XRD patterns of $N_1$-$NiS_2$-500 (a) and $N_3$-$NiS_2$-500 (b).

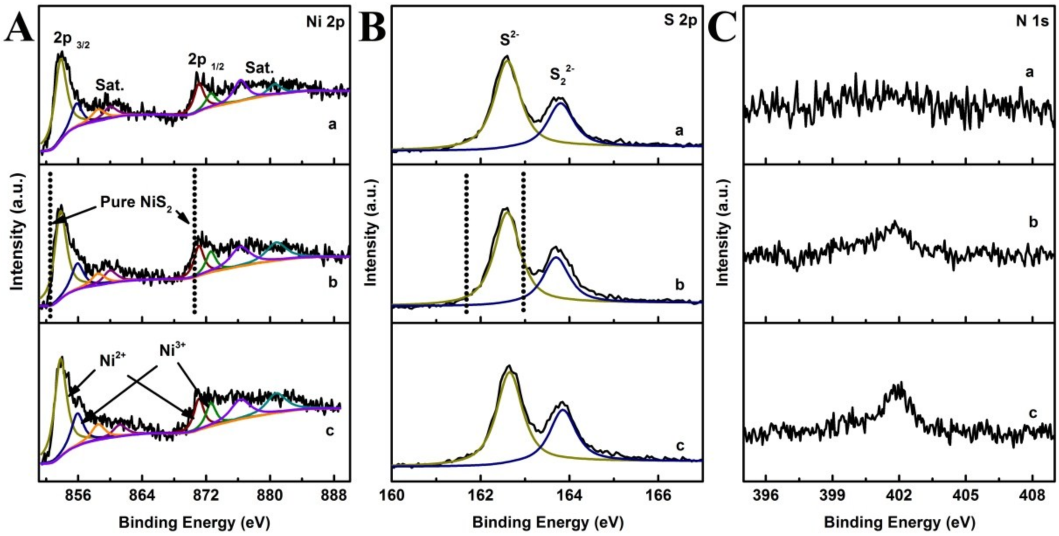


**Figure S5.** XPS spectra of $N_1$-$NiS_2$-500 (a), $N_2$-$NiS_2$-500 (b), and $N_3$-$NiS_2$-500 (c).

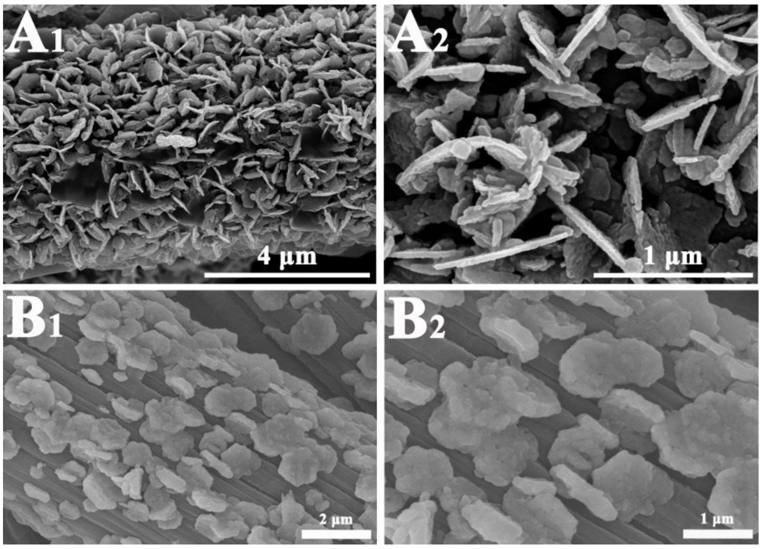


**Figure S6.** SEM images of $N_1$-$NiS_2$-500 (A) and $N_3$-$NiS_2$-500 (B).

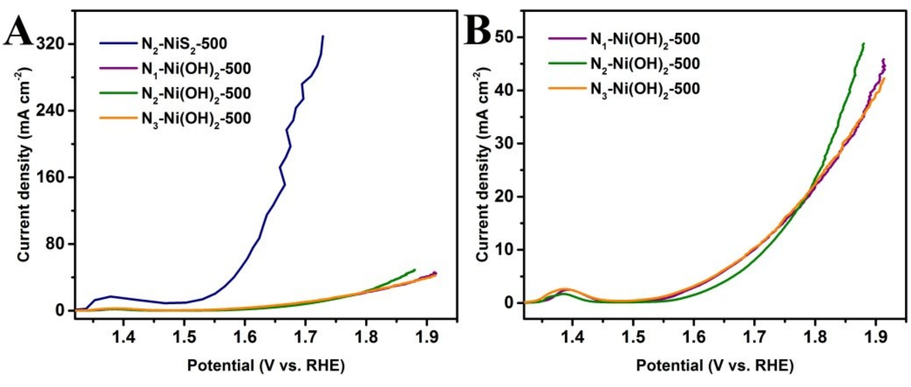


**Figure S7.** Polarization curves of $N_2$-$NiS_2$-500 and $Ni(OH)_2$ at higher (A) and (B) lower current density in 1.0 M KOH at a scan rate of 2 mV $s^{-1}$.

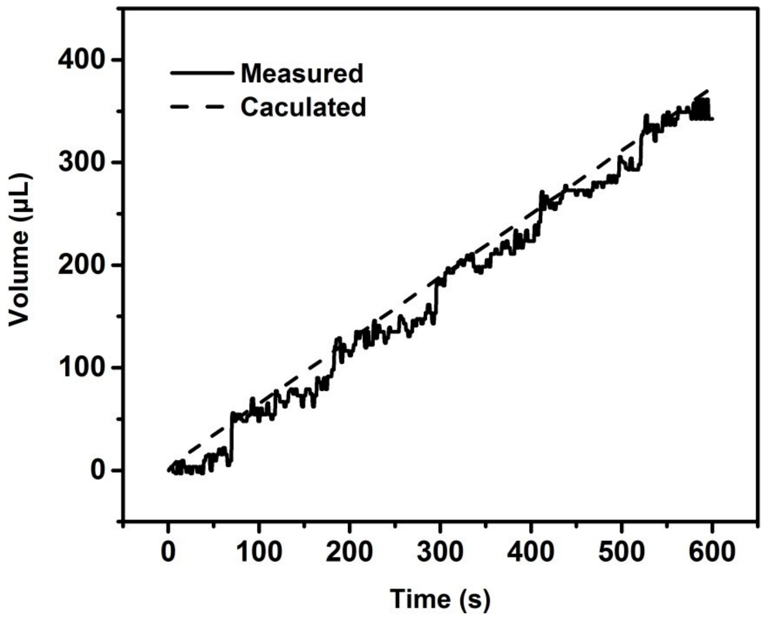


**Figure S8.** The theoretical and experimental amount of $O_2$ produced in potentiostatic electrolysis experiments (applied potential: 1.53 V for OER versus RHE).

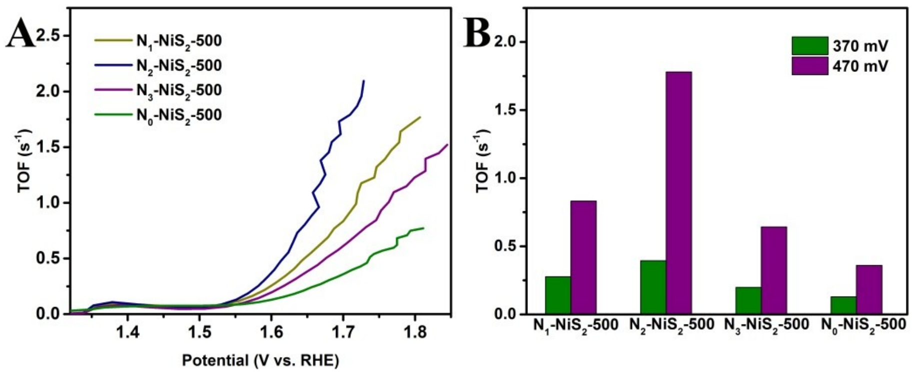


**Figure S9.** (A) Calculated TOF for N doped $NiS_2$. (B) The TOF obtained at different overpotentials.

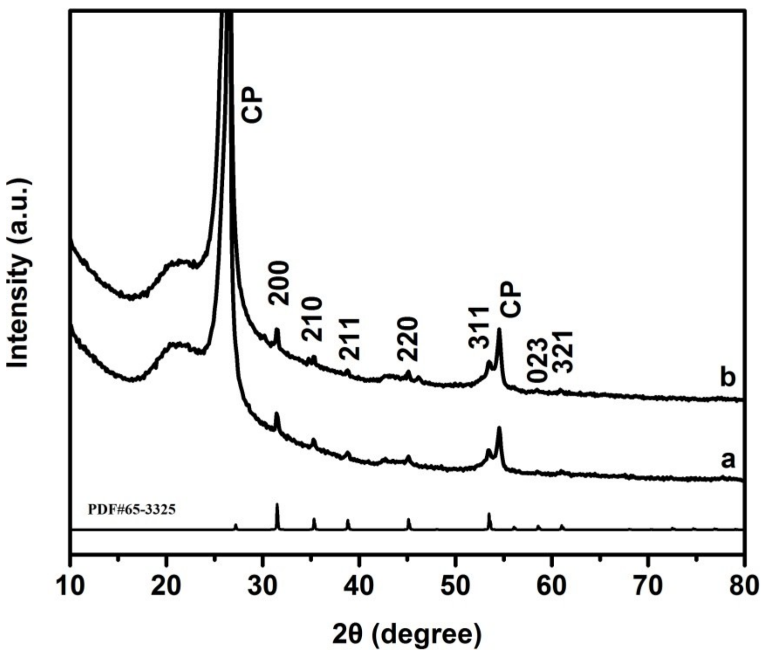


**Figure S10.** XRD patterns of $N_2$-$NiS_2$-400 (a) and $N_2$-$NiS_2$-600 (b).

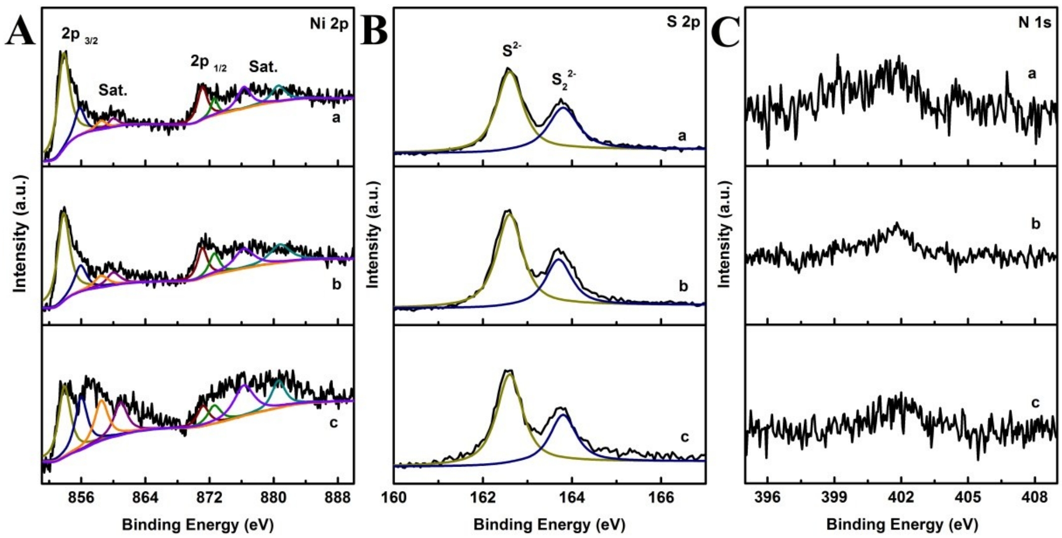


**Figure S11.** XPS spectra of $N_2$-$NiS_2$-400 (a), $N_2$-$NiS_2$-500 (b), and $N_2$-$NiS_2$-600 (c).

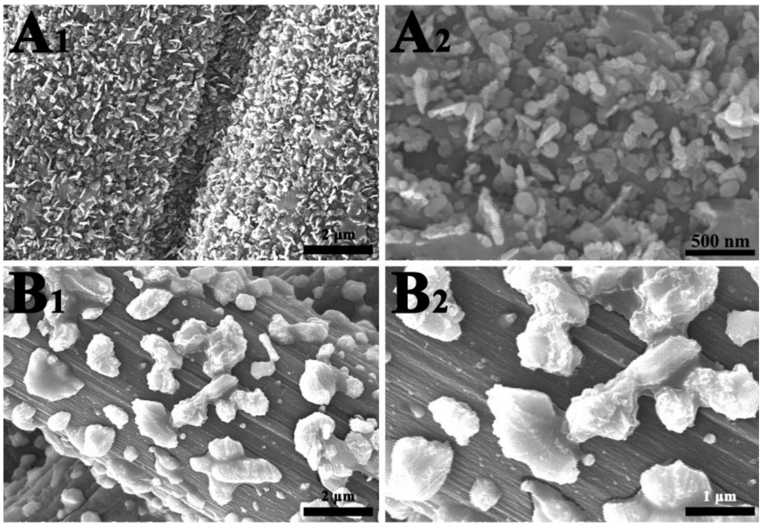


**Figure S12.** SEM images of $N_2$-$NiS_2$-400 (A) and $N_2$-$NiS_2$-600 (B).

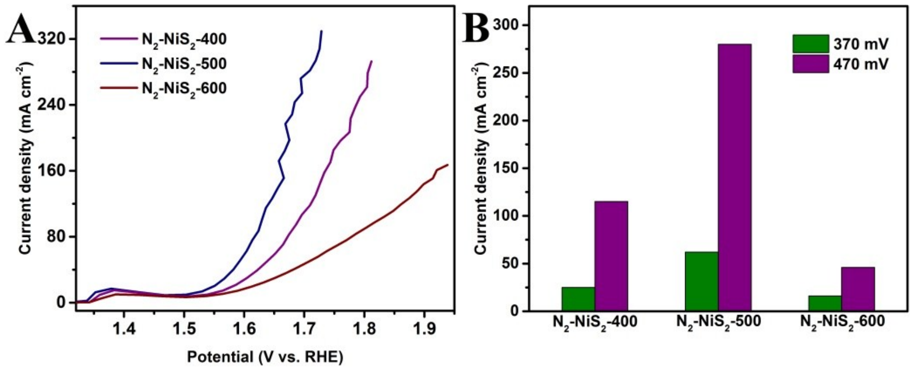


**Figure S13.** (A) Polarization curves of N doped $NiS_2$ in 1.0 M KOH at a scan rate of 2 mV $s^{-1}$ for OER. (B) The current density obtained at different overpotentials.

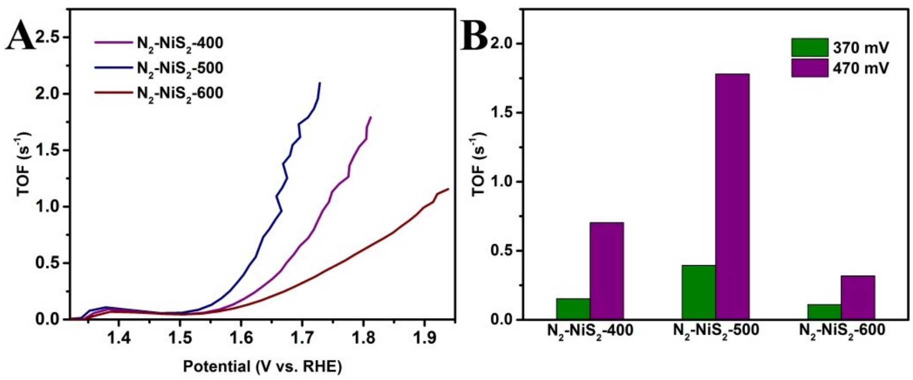


**Figure S14.** (A) Calculated TOF for N doped $NiS_2$. (B) The TOF obtained at different overpotentials.

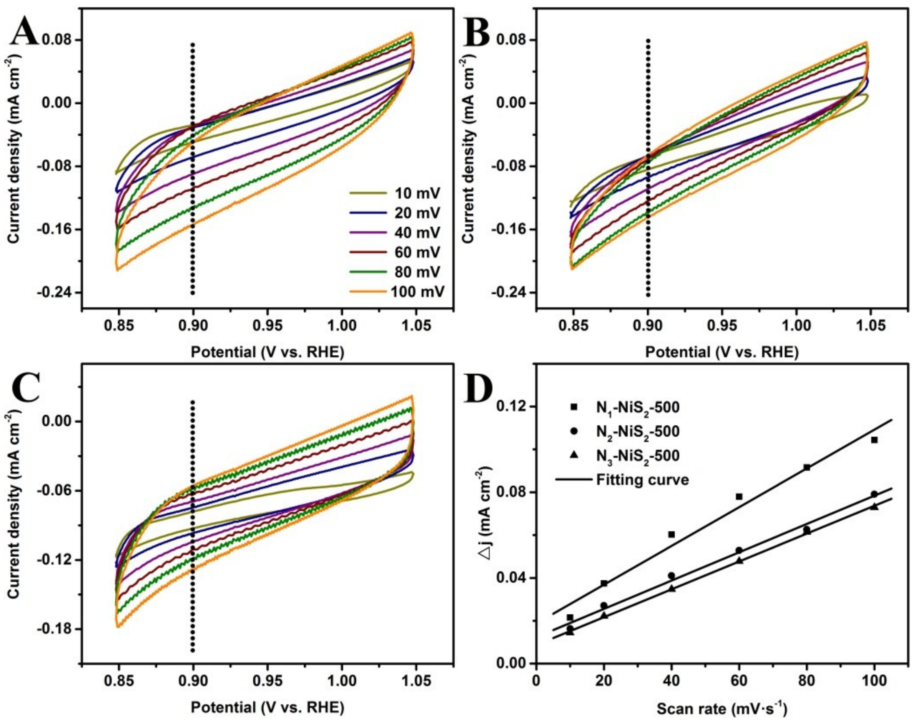


**Figure S15.** CV curves of $N_1$-$NiS_2$-500 (A), $N_2$- $NiS_2$-500 (B), and $N_3$- $NiS_2$-500 (C) at different scan rates. Current density differences (Δj) plotted against scan rates (D).

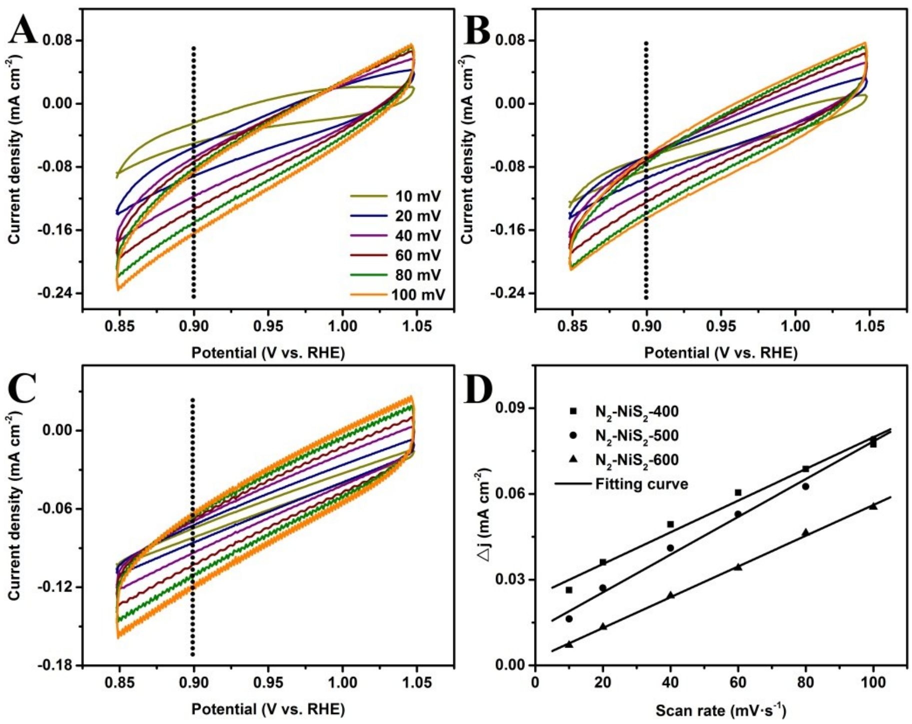


**Figure S16.** CV curves of $N_2$- $NiS_2$-400 (A), $N_2$- $NiS_2$-500 (B), and $N_2$- $NiS_2$-600 (C) at different scan rates. Current density differences (Δj) plotted against scan rates (D).

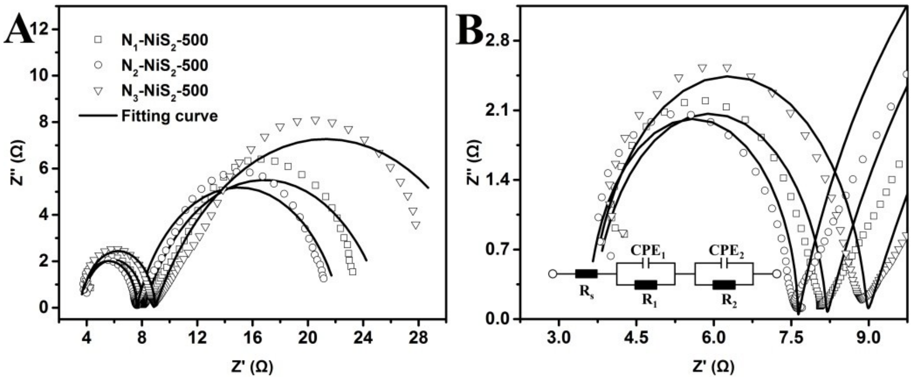


**Figure S17.** Nyquist plots of EIS spectra measured from $N_1$-$NiS_2$-500, $N_2$-$NiS_2$-500, and $N_3$-$NiS_2$-500.

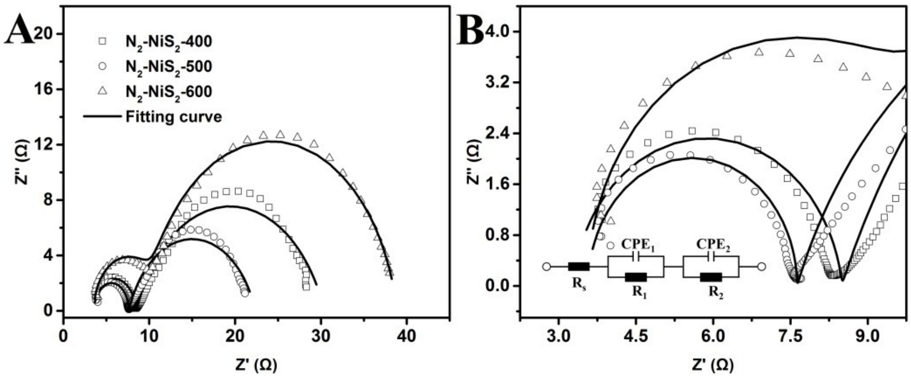


**Figure S18.** Nyquist plots of EIS spectra measured from $N_2$-$NiS_2$-400, $N_2$-$NiS_2$-500, and $N_2$-$NiS_2$-600.

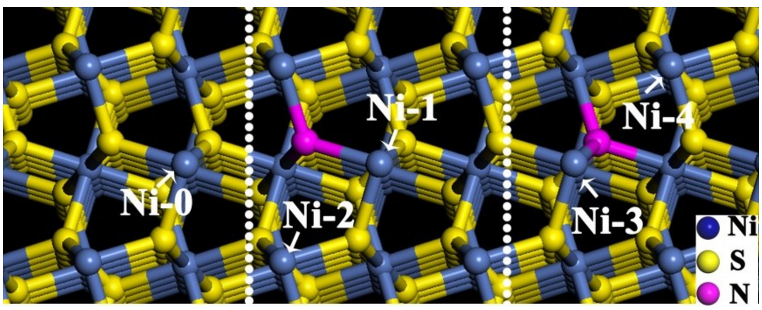


**Figure S19.** Possible absorption sites on the (001) $NiS_2$ and N doped $NiS_2$ surface.

**Table S1.** Nickel sulfide-based OER electrocatalysts and their performance.

| Electrocatalyst | Overpetential (mV)/ mA cm$^{-2}$ | Electrolyte solution | Ref. |
|---|---|---|---|
| $N_2$-$NiS_2$-500 | 270/$\eta_{10}$ | 1 M KOH | This work |
| $Ni_3S_2$/Ni foam | 310/$\eta_{10}$ | 0.1M KOH | 6 |
| $MoS_2$/$Ni_3S_2$ | 218/$\eta_{10}$ | 1M KOH | 7 |
| $NiS_2$/Ti foam | 330/$\eta_{10}$ | 1M KOH | 8 |
| High index $Ni_3S_2$ | 260/$\eta_{10}$ | 1M KOH | 9 |
| NiS@N/S-C | 417/$\eta_{10}$ | 1M KOH | 10 |
| NiS | 410/$\eta_{10}$ | 1M KOH | 11 |
| NiS Film | 320/$\eta_{10}$ | 1M KOH | 12 |
| NiS/ Ni foam | 335/$\eta_{50}$ | 1M KOH | 13 |
| Porous hollow NiS | 320/$\eta_{10}$ | 1M KOH | 14 |
| NiS@Stainless steel mesh | 297/$\eta_{10}$ | 0.1M KOH | 15 |
| h-NiSx/ Ni foam | 180/$\eta_{10}$ | 1M KOH | 16 |
| NiS/ Ni foam | 340/$\eta_{30}$ | 1M KOH | 17 |
| NiS Nanowire array | 300/$\eta_{10}$ | 1M KOH | 18 |

**Table S2.** OER electrocatalysts and their performance.

| Electrocatalyst | Overpetential (mV) at $\eta_{10}$ | Electrolyte solution | Ref. |
|---|---|---|---|
| $N_2$-$NiS_2$-500 | 270 | 1 M KOH | This work |
| FeCoW | 191 | 1M KOH | [19] |
| NiFe-LDH/CNTs | 247 | 1M KOH | [3] |
| FeCoW/Ni foam | 250 | 1M KOH | [20] |
| NiCoP/C | 330 | 1M KOH | [21] |
| $Co_4N$ | 257 | 1M KOH | [22] |
| Porous $MoO_2$ | 260 | 1M KOH | [23] |
| NiFe LDH | 260 | 1M KOH | [24] |
| Co-Fe-P | 280 | 1M KOH | [25] |
| $Co_3O_4$/CNTs | 290 | 0.1M KOH | [26] |
| $Ni_3Se_2$ | 290 | 0.3 M KOH | [27] |
| $NiCo_2O_4$ | 290 | 1M NaOH | [28] |
| CoN | 290 | 1M KOH | [29] |

**Table S3.** The fitting results of EIS spectra shown in Figure 17A and 18A using the equivalent circuit in their inset.

| Sample | $R_s$ (Ω) | $CPE_1$ ($F\cdot cm^{-2}$) | $n_1$ | $R_1$ (Ω) | $CPE_2$ ($F\cdot cm^{-2}$) | $n_2$ | $R_2$ (Ω) |
|---|---|---|---|---|---|---|---|
| $N_1$-$NiS_2$-500 | 3.66 | 6.44e$^{-7}$ | 0.94 | 4.52 | 0.055 | 0.72 | 17.35 |
| $N_2$-$NiS_2$-500 | 3.57 | 3.50e$^{-7}$ | 0.99 | 4.06 | 0.055 | 0.78 | 14.74 |
| $N_3$-$NiS_2$-500 | 3.61 | 5.52e$^{-7}$ | 0.94 | 5.36 | 0.042 | 0.68 | 24.69 |
| $N_2$-$NiS_2$-400 | 3.27 | 6.45e$^{-7}$ | 0.92 | 5.23 | 0.033 | 0.77 | 21.91 |
| $N_2$-$NiS_2$-600 | 3.55 | 2.40e$^{-7}$ | 0.98 | 6.29 | 9.64e-6 | 0.89 | 29.02 |

**Table S4.** The comparison of OER performance with different factors.

| Sample | $N_2$-$NiS_2$-500 | $N_1$-$NiS_2$-500 | $N_2$-$NiS_2$-400 | $N_3$-$NiS_2$-500 | $N_2$-$NiS_2$-600 |
|---|---|---|---|---|---|
| OER performance | +++++ | ++++ | +++ | ++ | + |
| Morphology | ++ | +++++ | ++++ | +++ | + |
| EASA | ++++ | +++++ | ++ | +++ | + |
| $R_2$ | +++++ | ++++ | +++ | ++ | + |
| $Ni^{3+}/Ni^{2+}$ | +++ | ++ | +++++ | ++++ | + |
| N content | +++++ (5.4%) | ++++ (4.8%) | +++ (3.6%) | ++ (3.1%) | + (2.3%) |

**Table S5.** $\Delta G$ of different sites.

| Site | Ni-0 | Ni-1 | Ni-2 | Ni-3 | Ni-4 |
|---|---|---|---|---|---|
| $\Delta G_a$ (eV) | 1.005 | 0.962 | 0.994 | 1.226 | 1.036 |
| $\Delta G_b$ (eV) | 2.411 | 2.007 | 2.417 | 0.890 | 1.974 |
| $\Delta G_c$ (eV) | 0.934 | 1.185 | 0.933 | 2.222 | 1.304 |
| $\Delta G_{*OH}$ (eV) | 1.005 | 0.961 | 0.994 | 1.226 | 1.036 |
| $\Delta G_{*O}$ (eV) | 3.416 | 2.968 | 3.410 | 2.116 | 3.010 |
| $\Delta G_{*OOH}$ (eV) | 4.350 | 4.153 | 4.344 | 4.338 | 4.314 |

## Reference


1. Z. Zhang, J. Hao, W. Yang and J. Tang, *RSC Adv*, 2016, **6**, 9647-9655.
2. Z. Huang, C. Lv, Z. Chen, Z. Chen, F. Tian and C. Zhang, *Nano Energy*, 2015, **12**, 666-674.
3. M. Gong, Y. Li, H. Wang, Y. Liang, J. Z. Wu, J. Zhou, J. Wang, T. Regier, F. Wei and H. Dai, *J Am Chem Soc*, 2013, **135**, 8452-8455.
4. S. J. Clark, M. D. Segall, C. J. Pickard, P. J. Hasnip, M. Probert, K. Refson and M. C. Payne, *Z Kristallogr*, 2005, **220**, 567-570.
5. J. Rossmeisl, A. Logadottir and J. K. Nørskov, *Chem Phys*, 2005, **319**, 178-184.
6. W. Zhou, X.-J. Wu, X. Cao, X. Huang, C. Tan, J. Tian, H. Liu, J. Wang and H. Zhang, *Energy Environ Sci*, 2013, **6**, 2921-2924.
7. J. Zhang, T. Wang, D. Pohl, B. Rellinghaus, R. Dong, S. Liu, X. Zhuang and X. Feng, *Angew Chem Int Ed*, 2016, **55**, 6702-6707.
8. N. Yang, C. Tang, K. Wang, G. Du, A. M. Asiri and X. Sun, *Nano Res*, 2016, **9**, 3346-3354.
9. L.-L. Feng, G. Yu, Y. Wu, G.-D. Li, H. Li, Y. Sun, T. Asefa, W. Chen and X. Zou, *J Am Chem Soc*, 2015, **137**, 14023–14026.
10. L. Yang, M. Gao, B. Dai, X. Guo, Z. Liu and B. Peng, *Electrochim Acta*, 2016, **191**, 813-820.
11. M. Gao, L. Yang, B. Dai, X. Guo, Z. Liu and B. Peng, *J Solid State Electrochem*, 2016, **20**, 2737-2747.
12. O. Mabayoje, A. Shoola, B. R. Wygant and C. B. Mullins, *ACS Energy Lett*, 2016, **1**, 195-201.
13. W. Zhu, X. Yue, W. Zhang, S. Yu, Y. Zhang, J. Wang and J. Wang, *Chem Commun*, 2016, **52**, 1486-1489.
14. P. Luo, H. Zhang, L. Liu, Y. Zhang, J. Deng, C. Xu, N. Hu and Y. Wang, *Acs Appl Mater Interfaces*, 2017, **9**, 2500-2508.

15. J. S. Chen, J. Ren, M. Shalom, T. Fellinger and M. Antonietti, *Acs Appl Mater Interfaces*, 2016, **8**, 5509-5516.
16. B. You and Y. Sun, *Adv Energy Mater*, 2016, **6**, 1502333.
17. G.-F. Chen, T. Y. Ma, Z.-Q. Liu, N. Li, Y.-Z. Su, K. Davey and S.-Z. Qiao, *Adv Funct Mater*, 2016, **26**, 3314-3323.
18. A. Sivanantham, P. Ganesan and S. Shanmugam, *Adv Funct Mater*, 2016, **26**, 4661-4672.
19. B. Zhang, X. Zheng, O. Voznyy, R. Comin, M. Bajdich, M. García-Melchor, L. Han, J. Xu, M. Liu, L. Zheng, F. P. García de Arquer, C. T. Dinh, F. Fan, M. Yuan, E. Yassitepe, N. Chen, T. Regier, P. Liu, Y. Li, P. De Luna, A. Janmohamed, H. L. Xin, H. Yang, A. Vojvodic and E. H. Sargent, *Science*, 2016, **352**, 333-337.
20. Y. Pi, Q. Shao, P. Wang, F. Lv, S. Guo, J. Guo and X. Huang, *Angew Chem*, 2017, **129**, 4573-4577.
21. P. He, X.-Y. Yu and X. W. Lou, *Angew Chem*, 2017, **129**, 3955-3958.
22. P. Chen, K. Xu, Z. Fang, Y. Tong, J. Wu, X. Lu, X. Peng, H. Ding, C. Wu and Y. Xie, *Angew Chem*, 2015, **127**, 14923–14927.
23. Y. Jin, H. Wang, J. Li, X. Yue, Y. Han, P. K. Shen and Y. Cui, *Adv Mater*, 2016, **28**, 3785–3790.
24. B. M. Hunter, J. D. Blakemore, M. Deimund, H. B. Gray, J. R. Winkler and A. M. Müller, *J Am Chem Soc*, 2014, **136**, 13118-13121.
25. A. Mendoza-Garcia, H. Zhu, Y. Yu, Q. Li, L. Zhou, D. Su, M. J. Kramer and S. Sun, *Angew Chem Int Ed*, 2015, **54**, 9642-9645.
26. T. Y. Ma, S. Dai, M. Jaroniec and S. Z. Qiao, *J Am Chem Soc*, 2014, **136**, 13925–13931.
27. A. T. Swesi, J. Masud and M. Nath, *Energy Environ Sci*, 2016, **9**, 1771-1782.
28. X. Gao, H. Zhang, Q. Li, X. Yu, Z. Hong, X. Zhang, C. Liang and Z. Lin, *Angew Chem Int Ed*, 2016, **55**, 6290-6294.
29. Y. Zhang, B. Ouyang, J. Xu, G. Jia, S. Chen, R. S. Rawat and H. J. Fan, *Angew Chem Int Ed*, 2016, **55**, 8670-8674.